Chapter 19
DOPPLER SONAR OBSERVATIONS OF LANGMUIR CIRCULATION

JEROME A. SMITH
Scripps Institution of Oceanography
La Jolla, California

19.1 Introduction

It has become increasingly clear that air-sea coupling is important to the earth's weather and climate [e.g., *Grotzner et al.* 1998, *Xu et al.* 1998]. The oceanic surface mixed layer is the link by which the air and sea are coupled. Further, the form and strength of the mixing motion are important to important concerns such as the fluxes of gases and nutrients and the growth and health of marine life. Improved understanding of all these processes depends in some measure on our understanding mechanisms and dynamics of the mixed layer.

One-dimensional "slab-models" of the mixed layer have performed remarkably well [e.g., *Pollard et al.* 1973, *Price et al.* 1986, *O'Brien et al.* 1991, *Large et al.* 1994, *Li et al.* 1995]. Under active mixing, the oceanic density profile erodes from the surface downward, producing a uniform layer over the remaining deeper profile. This mixed layer is approximately uniform in both velocity and density, with "jumps" occurring in both at the relatively sharp thermocline at the layer's base (like a "slab"). Horizontal gradients are assumed a priori to be of secondary importance. The erosion rate is then set to maintain a threshold value of the bulk Richardson number, depending only on the depth of the layer and the jumps in velocity and density at the base [*Pollard, et al.* 1973]. Some additional improvement is attained by permitting the erosion to penetrate smoothly into the thermocline over a depth proportional to the total mixed layer depth [*Large, et al.* 1994]. Additional deepening occurs when water at the surface is made denser by surface buoyancy fluxes; conversely, restratification occurs when heating

G. L. Geernaert (ed.), Air-Sea Exchange: Physics, Chemistry and Dynamics, 539-555.

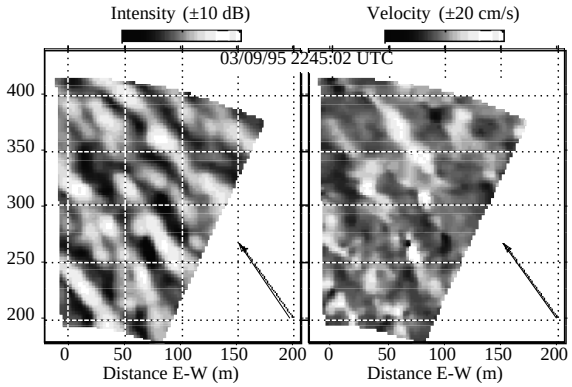

Figure 19.1 Example frame of PADS data: (left panel) Acoustic backscatter intensity; (right) Radial velocity. The arrows indicate wind speed and direction; the arrow shown represents a 15 m/s wind. North is up. The data are smoothed to 3 minute averages, modified to "track" the mean flow across the area.

exceeds mixing [*Price, et al.* 1986]. The velocity jump at the base of the mixed layer comes from inertial currents generated by the wind stress. Thus, while this bulk-shear mechanism is responsible for dramatically rapid initial deepening, it drops off near a quarter of an inertial day after the onset of wind, or in locations where inertial currents are suppressed.

Surface stirring by wind and waves can cause continued slower erosion [*Niiler and Krauss* 1977], and inhibits restratification. In its simplest form, the surface stirring is parameterized by a power of the wind friction velocity u^*; however, the multiplier best fitting the data varies from site to site. It is of interest to note two cases where these simple models deviate from the data: (1) [*O'Brien, et al.* 1991] note the failure of the real mixed layer to restratify as quickly as the model immediately after a rapid drop in wind; (2) *Li, et al.* [1995] note a tendency for the mixed layer depth to continue increasing slightly faster than the model with sustained winds. *Li, et al.* [1995, also *Li and Garrett* 1997] suggest that Langmuir circulation is responsible for the continued erosion, so deepening should depend on a combination of wave Stokes' drift and wind stress, as suggested by recent theories and models for the forcing of Langmuir circulation. Where waves are nearly fully developed the waves and wind is tightly coupled. In this case, scaling by the combined wind-wave term can be hard to separate statistically from just wind stress scaling (provided the magnitude of this stirring term is adjusted for the typical waves there). Notably, however, there are both places and times when the relation between wind and waves is not so direct. In particular, the anomalous mixing in "case 1" above occurs during a time of large waves and small stress, intimating that waves play an important role. It is suggested that wave climate variations cause the "stirring parameter" to vary.

Observations of the mixed layer often reveal coherent structures. These invite modeling with simplified dynamics, with hope of understanding their existence, behavior, and mixing efficiency. One such structure consists of horizontal rolls having

axes aligned with the wind, named "Langmuir circulation" in honor of their first categorical documentation [*Langmuir* 1938]. This is believed to dominate in wind mixing of the surface layer of lakes [*Langmuir* 1938], and is also important in the open ocean [*Weller et al.* 1985]. A mechanism for the generation of Langmuir circulation was identified in the late 1970s based on an interaction between waves and wind-driven currents [*Craik and Leibovich* 1976, *Garrett* 1976, *Craik* 1977, *Leibovich* 1977, *Leibovich* 1980]. The combination of an identifiable structure and a straightforward generation mechanism has energized modeling of the mixed layer. The catalytic effect is twofold: the mechanism provides a focus around which to build and refine models, and the structure provides a focus for comparison with observations.

To investigate the form and dynamics of wind-mixing at the surface of the ocean, observations of wind stress, waves, stratification, velocity profiles, and surface fields of radial velocity and acoustic backscatter intensity have been made over several month-long experiments during the past couple decades (Figure 19.1). In past experiments such as the Mixed Layer Dynamics Experiment (MILDEX) and the Surface Wave Processes Program (SWAPP), surface scattering Doppler sonar systems proved effective at measuring surface velocity and strain rates in a few isolated directions [*Smith et al.* 1987, *Smith* 1992, *Plueddemann et al.* 1996]. One interesting finding is that streaks associated with Langmuir cells sometimes split or coalesce [*Thorpe* 1992, *Farmer and Li* 1995, *Plueddemann, et al.* 1996], interpreted as vortex splitting or pairing. The one-dimensional views provided by single-beam sonars were ambiguous: the apparent time evolution of the pairing process could result either from time evolution of parallel features or from the lateral advection of essentially frozen Y-shaped features in a direction normal to the sonar beam. To resolve this, 2D spatial imaging is required. For example, *Farmer and Li* [1995] examined time series of acoustic intensity gathered with a mechanically scanning system, covering a full 360° circle every half minute or so, and verified that the Y junctions are, in general, spatial. [*Smith* 1998] analyzed images of backscatter intensity and radial velocity formed over a continuous sector. In contrast to the system employed by [*Farmer and Li* 1995], this "phased-array Doppler sonar" (PADS) system images the area simultaneously via digital beamforming, so that surface waves can be reliably averaged out, and the velocity estimates are statistically robust (see Figure 19.1). The latter data were gathered continuously, spanning several storms, so mixed layer evolution is unambiguously observed over all phases of storm and wave development.

Here, scaling of the surface motion associated with Langmuir circulation is sought as a function of wind, waves, and mixed layer depth (and additional parameters, if required). Surface velocities are derived from Doppler sonar measurements extending radially to as far as 450 m from the research platform *FLIP*, with 3 to 5 m spatial resolution. Averaging the data over 1 to 3 minutes filters out the surface waves, revealing patterns that are often elongated parallel to the wind (Figure 19.1). This permits continual assessment of strength, orientation, spacing, and degree of organization of the surface patterns, even when conditions are too rough for visual assessment. Of particular interest is the rms velocity scale V. Theoretical considerations suggest that surface velocity might scale roughly as $(u^* U^S)^{1/2}$, where u^*

is friction velocity and U^S the surface Stokes' drift due to the waves. However, as we shall see, the observations indicate that the surface velocity V scales with U^S alone within each well defined "wind event," once Langmuir circulation is established. The constant of proportionality varies significantly from one event to another, so that blindly averaging over several events destroys the correlation. This scaling suggests that (1) fully developed (nonlinear) Langmuir circulation does not scale the same way as initial growth, and (2) some additional variable is needed to parameterize this motion.

19.2 The Data.

Data from 2 field experiments are considered: the "Surface Waves Processes Program" (SWAPP), which took place some 300 km West of Pt. Conception, CA, in March of 1990, and leg 1 of the "Marine Boundary Layer Experiment (MBLEX), which took place 50 to 100 km offshore and just North of Pt. Conception (Figure 19.2). The former was undertaken with *FLIP* in a 3-point deep-ocean mooring, while in the latter *FLIP* was permitted to drift freely with the upper 90 m of the water column. In both, the surface velocities are estimated from surface-grazing acoustic Doppler sonar systems. In SWAPP, 4 discrete "inverted side-scan" style beams were used to trace the time-space evolution of features along 4 directions, distributed at 45° increments. In MBLEX, a newer system (PADS) was used to image a continuous area 35° in bearing by 450 m in range. Details concerning the former are found in [*Smith* 1992] and concerning the latter in [*Smith* 1998].

Wind and Stokes' drift are primary input parameters for models of Langmuir circulation. In both experiments, wind stress was estimated from sonic anemometer data via eddy-correlation methods. Stokes' drift was derived using data from resistance-wire wave arrays, yielding surface elevations and tilts as functions of frequencies up to 0.5 Hz [*Longuet-Higgins et al.* 1963]. The results are converted to Stokes' drift via linear theory and integrated over the directional-frequency spectrum to estimate the net drift at the surface. Additional details concerning instrumentation for SWAPP may be found in [*Smith* 1992], and for MBLEX in [*Smith* 1998]. The wind and Stokes' drift for MBLEX-1 are shown in Figure 19.3; those for SWAPP are shown in Figure 19.4. MBLEX-1 provided only one clear storm event. In SWAPP, 5 time segments were identified as encompassing potentially useful wind events. However, of these only the second and third segments have both steady wind directions and a wide range of wave age (segments are delineated in Figure 19.4 by different shades of gray; also denoted by the symbols * and + below the peaks in Stokes' drift).

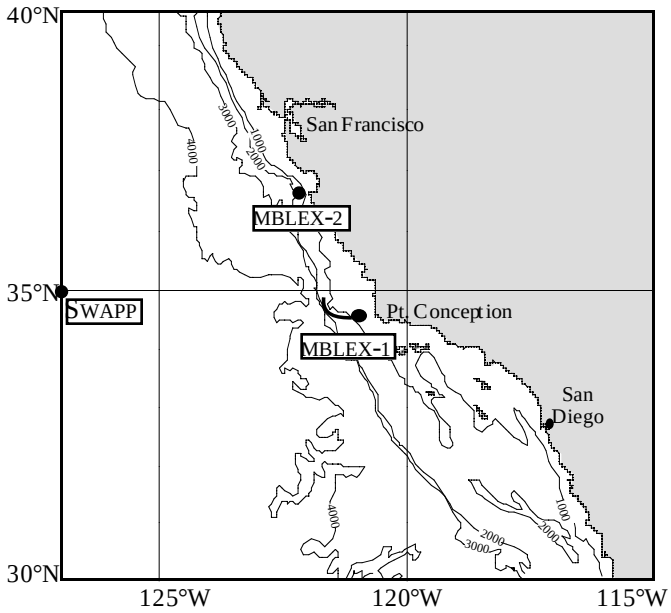

Figure 19.2 Locations of SWAPP and MBLEX experiments, showing (in particular) *FLIP's* drift-track over the most significant storm event in MBLEX-1.

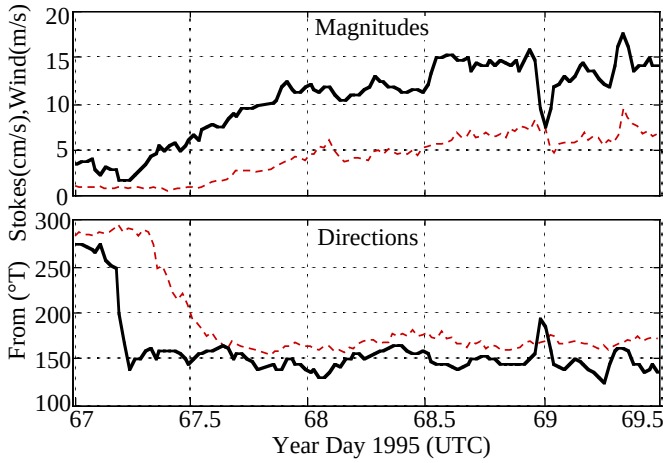

Figure 19.3 Wind (solid curve) and Stokes' drift (dashed curve) over the focus time segment of MBLEX leg 1. Note the delay between the onset of wind and development of Stokes' drift. Just prior to this segment, the wind was from the NW, and swell continued to come from that direction, explaining the slow reversal in Stokes' drift direction. Similar data were gathered for the SWAPP experiment.

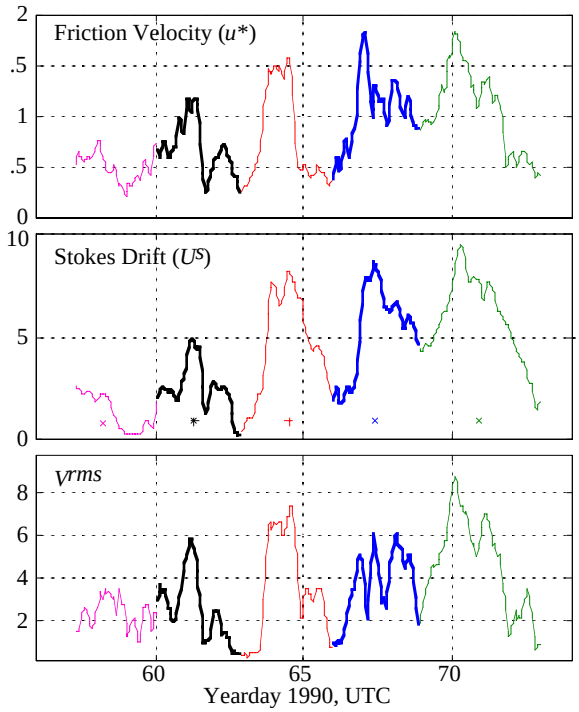

Figure 19.4 Wind, waves, and rms surface velocity during SWAPP. The first segment has weak variable winds; the last segment contains several directional shifts; the second-to-last segment has little variation in the ratio U^S/u^*. Thus, only the second and third segments are suitable for testing the relationship between the three parameters.

Stratification and the shear across the pycnocline are also primary input parameters to simple mixed layer models. In both experiments, stratification was monitored with rapid-profiling "Conductivity – Temperature – Depth" (CTD) systems, providing temperature and salinity profiles to 400 m depth every couple minutes. One useful summary parameter is the mixed layer depth "*h*," as shown (for example) in Figure 19.5 for the MBLEX data set. Vertical profiles of horizontal velocity were monitored with additional Doppler sonar systems in a standard Janus configuration. To estimate a "bulk shear," the surface velocities estimated from the surface sonar systems were used, together with velocity estimates averaged over a sub-thermocline depth interval of the standard Janus-type data.

19.3 Bulk Models and LC scaling.

To set the context for the following analysis of surface motion, and to help interpret the results, it's useful to review some simple ideas about wind mixing of the surface layer of an ocean. The MBLEX-1 event will be used for illustration. In the open ocean,

the largest effect is the shear across the thermocline, parameterized by a bulk Richardson number,

$$Ri \equiv \frac{\Delta\rho g h}{\rho_0 (\Delta U)^2} \geq 0.64 \text{ , or } \Delta\rho \geq 0.64(\Delta U)^2(\rho_o / gh) \qquad (19\text{-}1)$$

[*Pollard, et al.* 1973, *Price, et al.* 1986]. The velocity jump across the thermocline ΔU is primarily due to inertial currents generated by sudden changes in the wind; it therefore generally decreases rapidly after a quarter inertial cycle. The time history of the strength of this term is indicated in Figure 19.6 (thickest line) in terms of the $\Delta\rho$ needed across the thermocline to halt mixing (i.e., for the measured ΔU and mixed layer depth h). As shown in Figure 19.6 (thickest line), this term gets big quickly and then decays almost to zero over the next day. Since the wind rose gradually over the first day, the inertial currents were not as large as would have happened with a sudden wind turn-on. This is the essential explanation for the shallowness of the mixed layer in MBLEX-1, in spite of apparently strong forcing: the inertial current turned past 90° well before the maximum winds were reached.

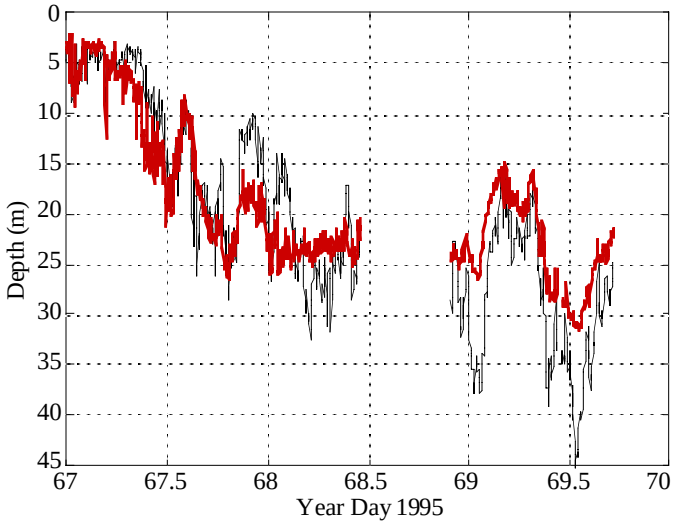

Figure 19.5 The mixed layer depth over the MBLEX-1 wind event, evaluated as the depth at which the temperature falls to 0.05°C below the value nearest the surface. The thin line shows "raw" mixed layer depth; the thick line is a psuedo-mixed-layer-depth from temperatures rescaled to constant heat capacity, compensating in part for vertical straining by low-mode internal waves or quasi-geostrophic motion.

After fast deepening by the PRT mechanism, surface stirring by wind and waves serves to maintain the mixed layer against restratification, and can also effect continued slow deepening [*Niiler and Krauss* 1977, *Li, et al.* 1995]. The parameterization of *Li et al.* incorporates scaling arguments appropriate to Langmuir circulation (i.e., a combination

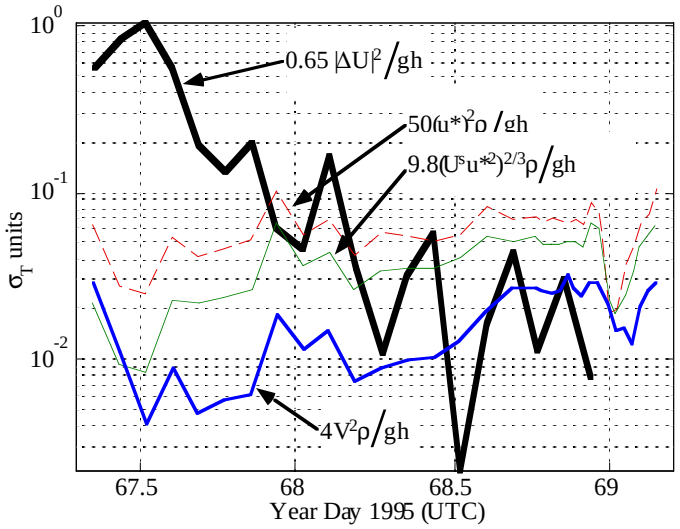

Figure 19.6 Mixing strength, parameterized by the density jump required to stop mixing, for (1) the bulk Richardson (or PRT) mechanism (thick line); (2) Langmuir circulation, as estimated directly from the rms velocity scale V (medium line); and (3) LC mixing estimated from U^S and ν_t via comparison with numerical model results, for developing waves (thin solid line) and for fully developed waves (thin dashed line).

of wind and wave velocity scales), although in the end they reduce the argument to a simple u^* dependence by assuming fully developed seas. For the sake of discussion, this latter parameterization is conceptually extended to underdeveloped waves.

The scaling suggested by *Li et al.* begins with the argument, derived from numerical modeling, that penetration into the thermocline is stopped if

$$\Delta\rho \geq 1.23\, w_{dn}^2 (\rho_o / gh)\,, \tag{19-2}$$

where w_{dn} is the maximum downwelling velocity associated with the Langmuir circulation. Using model results for w_{dn}, they rewrite this in the form

$$\Delta\rho \geq C u^{*2}\, (\rho_o / gh) \tag{19-3}$$

where

$$C \equiv 0.36\, U^s / k\nu_t\,, \tag{19-4}$$

in which ν_t is the turbulent kinematic eddy viscosity and k is the wavenumber of the dominant surface waves. For fully developed seas, they argue C is about 50 (Figure 19.6, thin dashed line). For illustration, this criterion is evaluated two additional ways: (1) extending the evaluation of C to underdeveloped waves, using estimates of U^S, k,

and ν_t in (19-4), and (2) using the rms horizontal scale (as described in next section) to estimate w_{dn} directly for use in (19-2).

To pursue the underdeveloped case, a significant requirement is estimation of ν_t. Recent dissipation measurements near the surface indicate that the turbulent velocity scale q is reasonable well described by the energy dissipation rate of the waves [*Terray et al.* 1996]. This, in turn, is well estimated by the energy input to the waves (within 7% or so). The growth rate β of a wave of radian frequency σ and phase speed c is approximately $\beta = 33\sigma(u*/c)^2$ [*Plant* 1982], so the net energy flux can be written in the form

$$q^3 \propto \rho^{-1}\beta E = 33ga^2\sigma(u*/c)^2 = 33(U^s u*^2)\,. \tag{19-5}$$

Conveniently, the final form in (19-5) remains approximately unchanged with integration over the wave spectrum (within a factor representing the typical directional spread). The length scale appropriate to wave breaking is proportional to the wave amplitude a, so we obtain an estimate of ν_t of the form $\nu_t \propto a(U^s u*^2)^{1/3}$. Substituting this into (19-4), and noting that ak in general does not vary significantly from about 0.1, we obtain

$$C \propto U^s/k\nu_t \propto (U^s/u*)^{2/3} \tag{19-6}$$

The values employed by *Li et al.* [1995] for fully developed waves imply $U^S/u* \rightarrow 11.5$. To obtain 50 with this value in (19-3), the constant of proportionality is set to 9.8. Then (19-6) becomes

$$\Delta\rho \geq 9.8(U^s u*^2)^{2/3}(\rho_o/gh)\,. \tag{19-7}$$

This criterion is also shown in Figure 19.6 (thin solid line).

To use the measured V^{rms} directly, we need to convert the horizontal rms to an estimate of maximum downwelling. Since the spacing is generally about twice the mixed layer depth, the rolls are roughly isotropic in the crosswind plane, and it's reasonable to set the vertical and crosswind velocity scales equal. Then the rms values must be translated into estimates of the maximum downwelling velocities. The circulation is not simply sinusoidal (in which case $w_{max} \sim 2^{1/2}V$) but varies somewhat randomly. By analogy to estimating significant wave height from the rms displacement, we set a threshold exceeded by 1/3 of all downwelling local maxima. This leads to a value roughly 2 times the rms. Hence we substitute $4V^2$ from the empirical rms velocity assessment (section 19.4) for w_{dn} in 2, as the direct estimate of the strength of mixing due to the observed Langmuir cells (Figure 19.6, lowest line).

The mixing effect estimated from the surface velocity measured in MBLEX-1 falls below the parametric estimates 3 and 7. As we shall see, the discrepancy is similar that between the observed velocity scales; the SWAPP variances agree more closely with these parameterizations. Over a period of several days, these differences could lead to

significant differences in the mixed layer depth. It is therefore important to understand how and why this variance is reduced.

19.4 Results: Scaling of Surface Motion.

The features observed at the surface can be characterized in terms of strength, spacing, orientation, and degree of organization. The objective here is to see whether the previously observed scaling for the strength (rms velocity) holds up over the combined data set. A subsidiary interest is to note the extent and limits to which intensity fluctuations compare to those of the dynamically more important velocity: can intensity images be used as a proxy for velocity in characterizing some aspects of the flow?

To estimate time series of the strength of variations in both intensity and radial velocity associated with Langmuir circulation, data averaged over 1 to 3 minutes were employed. The MBLEX-1 (PADS) data were averaged with a moving window that tracks the mean advection across the imaged area as the average is formed (see [*Smith* 1998] for details). The SWAPP data were processed with a dual spatial-temporal lag technique to isolate coherent signals while also tracking advection along the beam (see [*Plueddemann, et al.* 1996] or [*Smith* 1996] for details). The data were corrected for the spatial response of the instruments, estimated from simulated data. Strength is gauged by rms values. For radial velocity, the results are expressed in cm/s and denoted *V*. For intensity *I* they are expressed in rms decibels (dB). Log-intensity relative to the mean, corrected for beam pattern and attenuation, is used for two pragmatic reasons: (1) it makes the result independent of source loudness, and (2) the log-intensity is more nearly normally distributed, and so has better-behaved statistics.

Timeseries of intensity and velocity strengths for the MBLEX-1 event are shown in Figure 19.7. Both wind speed *W* and Stokes' drift U^S are also shown, scaled by constants chosen to yield reasonable fits to the rms velocities over the middle section of the time period. Streaks are first seen sometime after year day 67.7, as the wind exceeds 8 m/s. It is therefore reasonable to restrict the scaling analysis to the time segment after this. The strength scales of surface radial velocity features (or intensity) follow the Stokes' drift quite closely from year day 67.7 to the end of the segment, i.e., for winds over 8 m/s. The ratio of rms radial velocity (cm/s) to rms intensity (dB) remains close to 1.5 over the whole 44-hour period, indicating that similar information is obtained from either with respect to gross strength. Note, however, that near the end, when the wind suddenly drops (and veers momentarily by 60°), the intensity strength-scale drops by a larger fraction than velocity.

In the absence of wave forcing, the only relevant velocity scale would be the wind *W* (or friction velocity u^*; for present purposes, these are roughly proportional). Based on theories for initial growth of Langmuir circulation, it has been suggested that the cross-wind velocity fluctuations should scale roughly with either the geometric mean of the wind and Stokes' drift, $(WU^S)^{1/2}$ [*Plueddemann, et al.* 1996] or with $(W^2U^S)^{1/3}$

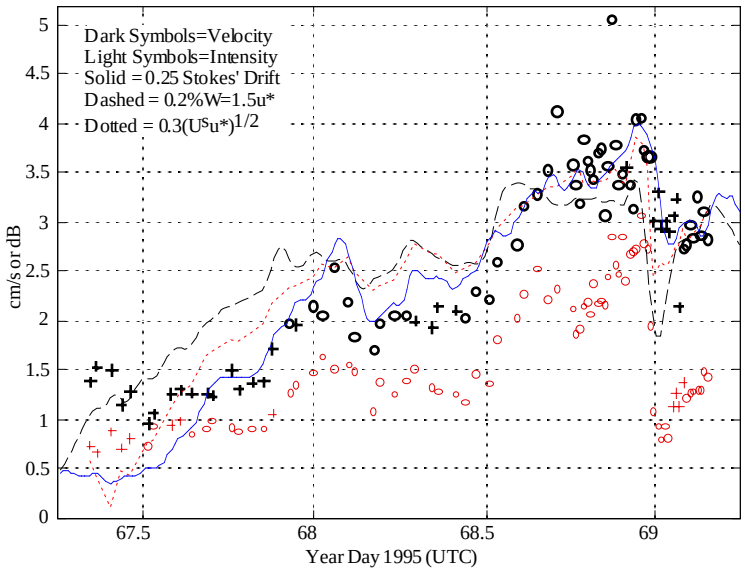

Figure 19.7 RMS radial velocity (dark symbols) and intensity (light symbols) associated with the features, versus time. Each symbol represents a half-hour average; crosses represent dubious estimates, circles more reliable ones. For scaling and comparison, $0.25U^S$ (solid line), $0.002W$ (dashed line), and $0.023(U^S W)^{1/2}$ (dotted line) are also shown.

[*Smith* 1996]. The suggested scalings for the surface velocity associated with Langmuir circulation can be cast in the general form $V \sim u^* (U^S/u^*)^n$. The value of n is then sought as the slope of the best fit line to $log_{10}(V/u^*)$ versus $log_{10}(U^S/u^*)$. The results for MBLEX-1 are reviewed in Figure 19.8; points where no surface stripes are visible are marked with +'s and excluded from the fit. Surprisingly, the value $n=1$ was found, with little uncertainty ($r^2=0.89$; error bounds on the slope are a standard deviation derived by the bootstrap method with 5000 trials, cf. [*Diaconis and Efron* 1983]). Note that U^S/u^* varies over almost an order of magnitude, and. In other words, once the Langmuir circulation is well developed, $V \sim U^S$, and wind stress no longer enters directly in scaling the motion. This implies a strong influence of the waves on the flow (and nonlinear, since a threshold must be applied for the existence of well-developed Langmuir circulation).

A natural question is whether this applies to other data, or is an isolated case. To this end, the SWAPP data were reanalyzed. Figure 19.4 shows the time-histories of wind, waves, and measured surface velocity scale from SWAPP. Figure 19.9 shows the log-log plot for all SWAPP and MBLEX data points, without regard for the existence of stripes or non-stationary conditions. It would be easy to dismiss any correlation from this plot; however, it should be recognized that (1) the parameter U^S might be a proxy for another wave parameter, and the relation between these might vary between wind events, and (2) there could be another parameter (or parameters) influencing the

relation. It is wise to examine the relation on a case-by-case basis, to see if there is a "hidden" relation. Unfortunately, as noted above, only events 2 and 3 of the potential 5 segments from SWAPP provide both a "clean" wind event (not confused by wind veering) and a wide range of U^S/u^*. These two events (henceforth "SWAPP-2" and "SWAPP-3") are plotted together with the "MBLEX-1" event in Figure 19.10. These regressions support the value n=1 for the exponent. Although the fits are not as tight as for the MBLEX-1 data, they are still statistically significant at well over 95%. Intriguingly, there is considerable offset between the lines, especially between SWAPP and MBLEX (by a factor of about 5), but also between the two SWAPP events (by a factor of about 2). Some other aspect of the environment must be affecting the relation.

What could be responsible for the observed variation in velocity scale V^{rms}? Possible candidates include variations of scaled depth of the mixed layer kh, effective viscosity ν_t, a directional effect of the horizontal Coriolis component [*Cox and Leibovich* 1997], or suppression by the buoyancy of the near-surface bubble cloud. A summary of some relevant parameters is given in Table 19.1. The first 6 parameters summarize the observations for the 3 events; the rest are derived from these. An effective wave period T^S is derived from the surface Stokes' drift, assuming the variations in mean-square wave steepness are not very large:

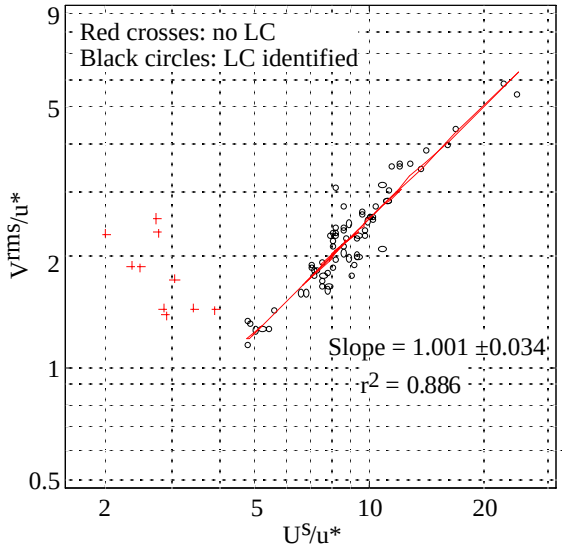

Figure 19.8 Scaling of the rms measured radial surface velocity takes the general form $V \sim u^*(U^S/u^*)^n$. The value of n is sought as the slope of (V/u^*) versus (U^S/u^*) on a log-log plot. This figure indicates a well-determined value for n very near 1.0; i.e., $V \sim U^S$, with no dependence on u^* once Langmuir circulation is well formed. Values before year day 67.66, when there were no signs of Langmuir circulation, are shown as red crosses but not included in the fit.

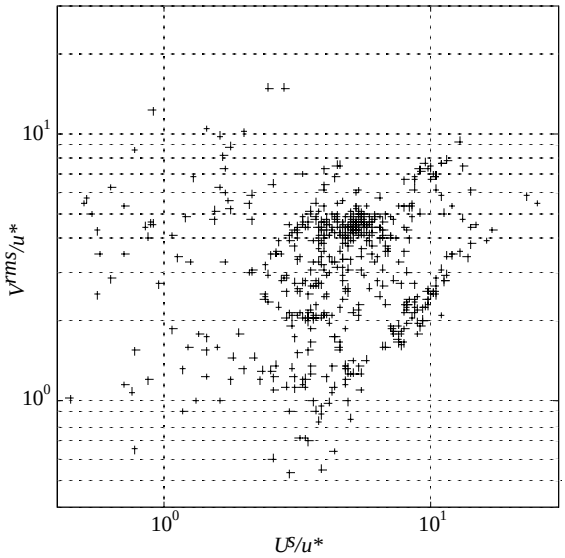

Figure 19.9 All data points from SWAPP and MBLEX-1, plotted without regard to event or whether LC features were identified. No correlation is seen, and it appears that almost an order of magnitude uncertainty in V^{rms} must be tolerated.

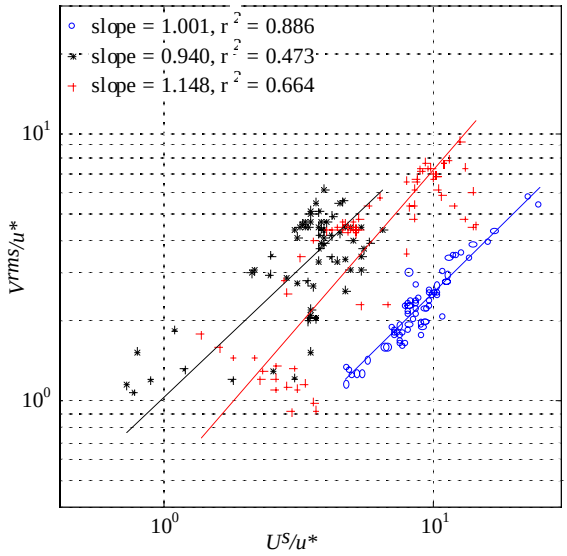

Figure 19.10 The empirical fits for *n* for each "good event" treated separately. Note that, within each event, the fit is fairly tight. However, the vertical offset of the lines varies significantly over just these three events.

$$U^S \approx \tfrac{1}{2}(ak)^2 c^p = T\,(ak)^2 g/4\pi \approx (const.)T \tag{19-8}$$

For the SWAPP-3 event, the peak wave period was estimated in a variety of ways [*Bullard and Smith* 1996], leading to a favored value of about 11.5 s near the end of the event; thus, we set the value of $(ak)^2$ by matching to that value in that event. The corresponding value for $(ak)^2$ is 0.0084, well within reason. The effective wavenumber is then computed from T^S via linear dispersion: $k^s = (2\pi/T^s)^2/g$. Given the uncertainty in defining a "peak period," and given the purported importance of wave Stokes' drift to the generation of Langmuir circulation, this proxy for the wave period and length scales appears to be most appropriate.

As reported in Table 19.1, the directions of MBLEX-1 and SWAPP-2 are similar, but the V-scaling differs by the largest ratio. This appears to rule out both the opposing swell and the horizontal Coriolis hypotheses. The estimated wave-induced viscosity is largest for SWAPP-3, but this is intermediate in V-scaling. Another possibility is suppression of motion by bubble buoyancy. The level of breaking presumably sets the overall density of the near surface bubble-cloud. A likely indicator of this is set by matching the rise-rate of the largest bubbles to the wave breaking turbulent velocity scale (as discussed above in connection with the turbulent eddy viscosity). Comparing this with the observed velocity scaling, it is seen that this parameter at least has the right ordering in magnitude, although the MBLEX-1 and SWAPP-3 values are relatively close. Finally, there is the "scale depth" kh of the mixed layer. It is important to distinguish here between the development of ΔV, V^{ms}, h, U^S, and k over the course of an event versus the differences between events. These all develop in parallel over the course of a wind event; however, what is of interest at the moment is whether they develop either at different rates or from different initial values between events. It is these latter differences between events that presumably set the ratio of V^{ms} to U^S over the event. Thus it is emphasized that this "scaled depth" refers to final or quasi-equilibrium values of h and k^S.

One way the scaled depth could influence the result is that the layer-averaged convergent force should be subtracted from the surface value, since this works to depress the thermocline rather than drive circulation. For roughly exponential decay with the depth-scale of the Stokes' drift, this leads to a net force at the surface reduced by the factor

$$F' = F_0 - \overline{F} \approx 1 - \tfrac{1}{h}\int_{-h}^{0} e^{-2kz}dz = 1-(2kh)^{-1}(1-e^{-2kh}) \tag{9}$$

Note that this varies smoothly from 0 at kh=0 to 1 as kh gets large; in other words, the wind-wave forcing mechanism is reduced for very thin layers, and reaches the full predicted strength as the mixed layer becomes deeper than the wave's scale-depth. As seen, the effect is in the right direction, but is again too weak to explain the full differences observed between the three events. It appears that further investigations are needed to select between the alternatives and to determine why and when suppression of the motion occurs.

Table 19.1 Various parameters that may influence the surface velocity scale.

Event	MBLEX-1	SWAPP-2	SWAPP-3
Parameter			
V^{rms}/U^S	0.25	0.95	0.67
W^{dir}	SE	SSE	NNW
W^{max}	15 m/s	10	13.6
u^*	1.65 cm/s	1.1	1.5
U^S	7.0 cm/s	4.5	7.5
h	25 m	25	45
T^S	10.7 s	6.9	11.5
k^S	0.035 m^{-1}	0.085	0.031
$k^S h$	0.87	2.12	1.37
F'	0.53	0.77	0.66
$(u^{*2}U^S)^{1/3}$	0.124 cm/s	0.082	0.119
ν_t	698 cm^2/s	190	770

19.5 Conclusions

The rms velocities associated with the low-frequency features appear to scale tightly with the Stokes' drift alone over the course of individual wind events, rather than with the wind or a combination of wind and waves. This relation is nonlinear in the sense that a threshold must be set for the existence of Langmuir circulation before it holds. Further, the "constant of proportionality" between surface velocity variance and Stokes' drift varies significantly between events. It is suggested that this is related to the ratio of wavelength to mixed layer depth, as parameterized by the "final" or maximal values. Dynamic effects of the near-surface bubble layer could also play a role.

In each event considered here, the mixed layer deepened rapidly, then remained fairly constant, with very slow (if any) continued erosion. This is consistent with current thinking, where the "bulk dynamics" of shear across the thermocline due to inertial motion is the primary agent for deepening in the open ocean. Surface stirring by the combined action of wind and waves may help maintain the mixed layer after this, and may induce additional slow deepening. In any case, the inertial current "bulk Richardson number" mechanism is the lowest order term in wind-induced mixing of the surface layer.

Overall strength correlates well between intensity and velocity features over longer timescales. However, in details such as spacing, orientation, or short-time behavior, significant differences occur. The time/space-dependent behavior of bubbles in a time-varying flow should be investigated. Simulations with realistic bubble dynamics may help to understand these differences.

19.6 Acknowledgments.

Thanks are due to the many people involved in both SWAPP and MBLEX. Regarding the gathering of this data, thanks go especially to Eric Slater, Lloyd Green, Mike Golden, Chris Neely, R. Pinkel, K. Rieder, M. Alford, and to the crew of the research platform *Flip*, captained by E. DeWitt (SWAPP) and T. Golfinas (MBLEX). Thanks also

for useful comments from R. Pinkel, C. Garrett, and G. Terray. This work was supported by the Office of Naval Research, grants N00014-93-1-0359 and N00014-96-1-0030.

References

Bullard, G. T., and J. A. Smith, Directional spreading of growing surface waves, in *The air-sea interface: radio and acoustic sensing, turbulence and wave dynamics*, Edited by M. A. Donelan, W. H. Hui, and W. J. Plant, pp. 311-319, The Rosenstiel Scholl of Marine and Atmospheric Science, Miami, FL, 1996.

Cox, S. M., and S. Leibovich, Large-scale three-dimensional Langmuir circulation, *Physics of Fluids*, *9*, 2851-2863, 1997.

Craik, A. D. D., The generation of Langmuir circulation by an instability mechanism, *J. Fluid Mech.*, *81*, 209-223, 1977.

Craik, A. D. D., and S. Leibovich, A rational model for Langmuir circulations, *J. Fluid Mech.*, *73*, 401-426, 1976.

Diaconis, and B. Efron, Computer-intensive methods in statistics, *Sci. Am.*, *248*, 116-130, 1983.

Farmer, D., and M. Li, Patterns of bubble clouds organized by Langmuir circulation, *J. Phys. Oceanogr.*, *25*, 1426-1440, 1995.

Garrett, C., Generation of Langmuir circulations by surface waves– A feedback mechanism, *J. Mar. Res.*, *34*, 117-130, 1976.

Grotzner, A., M. Latif, and T. P. Barnett, A decadal climate cycle in the North Atlantic Ocean as simulated by the ECHO coupled GCM, *Journal of Climate*, *11*, 831-847, 1998.

Langmuir, I., Surface motion of water induced by wind, *Science*, *87*, 119-123, 1938.

Large, W. G., J. C. McWilliams, and S. C. Doney, Oceanic vertical mixing: A review and a model with a nonlocal boundary layer parameterization, *Rev. Geophys.*, *32*, 363-403, 1994.

Leibovich, S., Convective instability of stably stratified water in the ocean, *J. Fluid Mech.*, *82*, 561-581, 1977.

Leibovich, S., On wave-current interaction theories of Langmuir circulations, *J. Fluid Mech.*, *99*, 715-724, 1980.

Li, M., and C. Garrett, Mixed layer deepening due to Langmuir circulation, *J. Phys. Oceanogr.*, *27*, 121-132, 1997.

Li, M., K. Zahariev, and C. Garrett, Role of Langmuir circulation in the deepening of the ocean surface mixed layer, *Science*, *270*, 1955-1957, 1995.

Longuet-Higgins, M. S., D. E. Cartwright, and N. D. Smith, Observations of the directional spectrum of sea waves using the motions of a floating buoy, in *Ocean Wave Spectra: Proceedings of a Conference*, Edited by National Academy of Sciences, pp. 111-132, Prentice-Hall, Englewood Cliffs, N.J., 1963.

Niiler, P. P., and E. B. Krauss, One-dimensional models of the upper ocean, in *Modeling and Prediction of the Upper Layers of the Ocean*, Edited by E. B. Krauss, pp. 143-172, Pergammon, Tarrytown, N. Y., 1977.

O'Brien, M. M., A. Plueddemann, and R. A. Weller, The response of oceanic mixed layer depth to physical forcing - modelled vs observed, *Biol. Bull.*, *181*, 360-361, 1991.

Plant, W. J., A relationship between wind stress and wave slope, *J. Geophys. Res.*, *87*, 1961-1967, 1982.

Plueddemann, A. J., J. A. Smith, D. M. Farmer, R. A. Weller, W. R. Crawford, R. Pinkel, S. Vagle, and A. Gnanadesikan, Structure and variability of Langmuir circulation during the surface waves processes program, *J. Geophys. Res.*, *101*, 3525-3543, 1996.

Pollard, R. T., P. B. Rhines, and R. Thompson, The deepening of the wind-mixed layer, *Geophys. Fluid Dyn.*, *4*, 381-404, 1973.

Price, J. F., R. A. Weller, and R. Pinkel, Diurnal cycling: Observations and models of the upper ocean response to diurnal heating, cooling, and wind mixing, *J. Geophys. Res.*, *91*, 8411-8427, 1986.

Smith, J. A., Observed growth of Langmuir circulation, *J. Geophys. Res.*, *97*, 5651-5664, 1992.

Smith, J. A., Observations of Langmuir circulation, waves, and the mixed layer, in *The Air Sea Interface: Radio and Acoustic Sensing, Turbulence, and Wave Dynamics*, Edited by M. A. Donelan, W. H. Hui, and W. J. Plant, pp. 613-622, Univ. of Toronto Press, Toronto, Ont., 1996.

Smith, J. A., Evolution of Langmuir circulation during a storm, *Journal of Geophysical Research*, *103*, 12,649-12,668, 1998.

Smith, J. A., R. Pinkel, and R. Weller, Velocity structure in the mixed layer during MILDEX, *J. Phys. Oceanogr.*, *17*, 425-439, 1987.

Terray, E. A., M. A. Donelan, Y. C. Agrawal, W. M. Drennan, K. K. Kahma, A. J. Williams, P. A. Hwang, and S. A. Kitaigorodskii, Estimates Of Kinetic Energy Dissipation Under Breaking Waves, *Journal Of Physical Oceanography*, *26*, 792-807, 1996.

Thorpe, S. A., The breakup of Langmuir circulation and the instability of an array of vortices, *J. Phys. Oceanogr.*, *22*, 350-360, 1992.

Weller, R., J. P. Dean, J. Marra, J. Price, E. A. Francis, and D. C. Boardman, Three-dimensional flow in the upper ocean, *Science*, *227*, 1552-1556, 1985.

Xu, W., T. P. Barnett, and M. Latif, Decadal variability in the North Pacific as simulated by a hybrid coupled model, *Journal of Climate*, *11*, 297-312, 1998.